

## Chaos-assisted tunneling with cold atoms

A. Mouchet,<sup>1,\*</sup> C. Miniatura, R. Kaiser,<sup>2,†</sup> B. Grémaud, and D. Delande<sup>3,‡</sup>

<sup>1</sup>*Laboratoire de Mathématiques et de Physique Théorique (CNRS UPRES-A 6083), Avenue Monge, Parc de Grandmont, 37200 Tours, France*

<sup>2</sup>*Laboratoire Ondes et Désordre (CNRS FRE 2302), 1361 route des Lucioles, Sophia Antipolis, F-06560 Valbonne, France*

<sup>3</sup>*Laboratoire Kastler-Brossel (CNRS UMR 8552), Université Pierre et Marie Curie, 4 place Jussieu, F-75005 Paris, France*

(Received 7 December 2000; published 26 June 2001)

In the context of quantum chaos, both theory and numerical analysis predict large fluctuations of the tunneling transition probabilities when irregular dynamics is present at the classical level. Here we consider the nondissipative quantum evolution of cold atoms trapped in a time-dependent modulated periodic potential generated by two laser beams. We give some precise guidelines for the observation of chaos-assisted tunneling between invariant phase space structures paired by time-reversal symmetry.

DOI: 10.1103/PhysRevE.64.016221

PACS number(s): 05.45.Mt, 05.60.Gg, 32.80.Qk, 05.45.Pq

### I. INTRODUCTION

During the 1970's and 1980's it gradually became clear that classical Hamiltonian chaos profoundly affects the temporal evolution and spectral properties of the corresponding quantum system as compared to the integrable case [1]. Some of these features (dynamical localization, scars of periodic orbits [2], etc) share striking similarities with concepts originating from condensed matter physics such as weak and strong localization [3]. In fact these phenomena can be recast in terms of wave transport in disordered media, the (quasi) randomness being of statistical or dynamical origin. In this context, it is important to understand the mechanisms underlying a key feature of wave propagation which has no classical analog: tunneling.

Tunneling refers to any wave process which is classically forbidden to *real* solutions of the Hamilton equations. For one-dimensional (1D) autonomous systems, it is well known that the quantum tunneling probability through an energetic barrier can be evaluated semiclassically with the help of classical *complex* solutions of the Hamilton equations [4,5]. The direct generalization of this procedure to higher dimensional systems is straightforward for separable dynamics, but is already subtle for integrable, but no longer separable, dynamics [6,7]. In the generic case of chaotic dynamics, it even proves extremely hard to handle, and the situation, until recently, seemed hopeless. Indeed, in the presence of chaos, the analytical and topological properties of the classical *complexified* phase space are far from trivial. During the last ten years however, theoretical and numerical investigations on autonomous 2D and time-dependent 1D Hamiltonian systems have started to highlight some mechanisms [6–12], and much insight has been gained on the influence of such classical nonseparable dynamics. Experimental evidence of such mechanisms, which is still lacking, would be of great interest especially in the light of the subtle interplay between interferences and disorder.

In this paper, we consider 1D time-dependent dynamics, one of the simplest cases where irregular motion can appear, and we study chaos-assisted tunneling. Our effective Hamiltonian model, which is derived from an experimentally achievable situation, exhibits three main properties. First, its classical dynamics is invariant under time reversal. Second it is controlled by a single real external parameter  $\gamma$  (for  $\gamma = 0$  the dynamics is integrable and chaos develops more and more in phase space as  $\gamma$  is increased). Third, there exists in phase space, for a whole continuous range of  $\gamma$ , a pair of stable islands  $\mathcal{I}_+$  and  $\mathcal{I}_-$  which are time-reversed images of each other. By stable islands we mean the set of regular classical trajectories in phase space which stay near a stable equilibrium point or near a stable periodic orbit of the system. In this case, no real classical orbit started in one of these islands can go into the other one. However, the quantum dynamics of a wave packet, initially prepared in one island, will display a periodic behavior. The wave packet oscillates from one island to its time-reversed image [13]. In the quantum spectrum this tunneling process appears via the existence of nondegenerate energy doublets whose splitting gives the inverse of the tunneling time between  $\mathcal{I}_+$  and  $\mathcal{I}_-$ . Varying  $\gamma$  slowly modifies the geometry of the islands themselves. The crucial point is that it will drastically change the classical dynamics for some initial conditions lying between the islands. For small enough  $\gamma$ , the chaotic layers are too small to play a significant role at  $\hbar$  scales, and hence cannot influence the quantum behavior of the system, which is essentially still regular. For larger values, but still before the stable islands are completely destroyed, there is a chaotic regime where varying  $\gamma$  or  $\hbar$  ( $\hbar$  being in this case Planck's constant divided by some typical classical action) alone induces large fluctuations, of several orders of magnitude, of the doublet splittings around their mean value. This in turn corresponds to large fluctuations of the tunneling periods. These large fluctuations, induced by small changes of any parameter, are a signature of the so-called “chaos-assisted tunneling” regime. This has been extensively studied both theoretically and numerically in the situation described above [8–11], but has not yet been observed in real experiments, the main reason being its extreme sensitivity to small changes in the classical dynamics. Any *uncontrolled* varia-

\*Electronic address: mouchet@celfi.phys.univ-tours.fr

†Electronic address: miniat,kaiser@inln.cnrs.fr

‡Electronic address: gremaud,delande@spectro.jussieu.fr

tion of  $\gamma$ , be it noise or dissipation, will dramatically wash out or destroy the signal. The observation of this highly fluctuating tunneling regime thus requires both an accurate control of the dynamics of the preparation of the initial state and of the analysis of the final state. The observation of doublet splittings is rather common in molecular physics, when a discrete symmetry like parity is present. In most cases, the splitting is due to standard tunneling either through an energy barrier or a dynamical barrier (see, for example, Refs. [15–17]). It was suggested in some cases [18,19] that this splitting is influenced by the existence of chaos in the classical dynamics. Thus molecular physics provides us with systems where chaos-assisted tunneling could be experimentally observed. However, one usually lacks an external parameter which could allow for the observation of the fluctuations of the tunneling rate.

Atom cooling techniques [14] provide systems which fulfill all the desired requirements. They allow an accurate manipulation and control of internal and external degrees of freedom, and are a useful tool to produce situations where the wave character of the atomic motion is essential [20]. A great variety of interaction potentials can be produced to influence the atomic motion, be it by means of inhomogeneous magnetic fields, material gratings, or laser light. Optical lattices with crystalline or quasicrystalline order [21–23] can be easily produced where atoms mimic situations usually encountered in condensed matter [24,25]. Dissipation (spontaneous emission and atom-atom interaction) is easily controlled, and coherence times of the order of 10 ms can readily be achieved. This is why cold atoms are a unique tool to study transport properties of waves, be it quantum chaos [26] or weak localization [27,28].

This paper is organized as follows. In Sec. II we explain the origin of the effective Hamiltonian for the experimental situation under consideration. In Sec. III we study the corresponding classical dynamics, and show why this effective Hamiltonian is relevant for chaos assisted tunneling. In Sec. IV we quickly review some of the usual theoretical techniques when dealing with both space and time periodic quantum dynamics. We also illustrate how some quantum spectral properties have a natural classical interpretation. In Sec. V we show, with the help of numerical experiments, how chaos-assisted tunneling arises in our system, and then explain how to observe it in a real experiment. Section VII is devoted to some concluding remarks.

## II. EFFECTIVE HAMILTONIAN

### A. Light shifts

The very basic physical mechanism underlying our forthcoming discussion is the following: when an atom is exposed to monochromatic light, its energy levels are shifted by the interaction. These level shifts originate from the polarization energy of the atom in the incident light field, and are called light shifts [29]. In the dipolar approximation, they depend on the field intensity value at the center-of-mass position of the atom. If the field intensity is space-time dependent, then a moving atom will experience dipolar forces: inhomogeneous light shifts result in forces and alter the center-of-mass

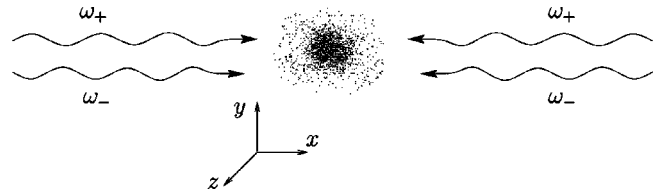


FIG. 1. Experimental configuration under consideration: a cloud of two-level atoms is illuminated by two monochromatic standing waves with frequencies  $\omega_{\pm} = \omega_L \pm \delta\omega/2$  ( $\delta\omega \ll \omega_L$ ). All fields are linearly polarized along the same direction, and are sufficiently far detuned from the atomic resonance so that dissipation effects can be ignored.

motion of the atom. By appropriately tailoring the space-time dependence of the light field, one can then produce a great variety of potentials for the external atomic motion, as proven by the atom cooling community. Note, however, that the atom-light interaction is also responsible for a dissipative phenomenon (real absorption of a photon followed by spontaneous emission) which shortens the temporal coherence of the atomic wave function. By using a laser light far detuned from any atomic resonance, it is possible to control this stray phenomenon and maintain it at a reasonably low rate. In the following, we shall describe a simple physical situation for atoms where chaos-assisted tunneling is expected to be present.

### B. Experimental configuration

Although the internal structure (hyperfine Zeeman sublevels) are of major importance in atom cooling, here, for simplicity, we will model the atom by a two-level system (as only one optical transition usually governs the dynamics). We consider a dilute sample of identical (but independent) two-level atoms propagating in the light field configuration created by two monochromatic standing waves with frequencies  $\omega_{\pm} = \omega_L \pm \delta\omega/2$  where  $\delta\omega \ll \omega_L$ . We denote the groundstate and excited state of each atom by  $|g\rangle$  and  $|e\rangle$ , these levels being connected by an electric dipole transition of angular frequency  $\omega_{at}$  and width  $\Gamma$ . All atoms are supposed to be initially prepared in their ground state. Each standing wave is produced along the  $x$  axis by two counter-propagating laser beams, and we suppose all fields to be linearly polarized along the  $z$  axis (see Fig. 1). After a suitable choice of space-time origin, the total electrical field strength is

$$E(x,t) = [E_+ \cos(\omega_+ t) + E_- \cos(\omega_- t)] \cos(k_L x), \quad (1)$$

where  $E_{\pm}$  are the field strengths of the two standing waves. At this point we have neglected the difference in wave vectors of the standing waves. For this to hold, it is sufficient to assume that the atomic sample size is small enough. Typically, the difference in the  $k$  vectors will be of the order of  $10^{-9}$  or less (see below), so that this requires the atomic cloud to be smaller than typically a few kilometers, which is amply satisfied in a standard magneto-optical trap.

### C. Dimensionless effective Hamiltonian

The effective Hamiltonian which describes the atomic motion is derived in Appendix A under some common and well-controlled approximations. It acts in the Hilbert space of a one-dimensional system which is simply the  $x$  component (position) of the center of mass of the atom (which means that the internal degree of freedom as well as the  $y$  and  $z$  coordinates can be eliminated; see Appendix A). This reads

$$H = \frac{p_x^2}{2M} - V_0 \cos(2k_L x) [\theta + \cos(\delta\omega t)], \quad (2)$$

where  $V_0 \stackrel{\text{def}}{=} -\hbar\Omega_+ \Omega_- / 8\delta_L$  and  $\theta \stackrel{\text{def}}{=} (\Omega_+ / 2\Omega_-) + (\Omega_- / 2\Omega_+)$ , with  $\delta_L = \omega_L - \omega_{at}$  the detuning with respect to the atomic frequency and  $\Omega_{\pm} = dE_{\pm} / \hbar$  ( $d$  being the atomic dipole strength). Without loss of generality we will assume  $V_0$  to be positive since, if  $V_0$  is negative, it is sufficient to shift  $x$  by  $\pi/2k_L$  to recover this case.

In the following, it will prove convenient to work with dimensionless quantities. Rescaling quantities through  $\tau \stackrel{\text{def}}{=} \delta\omega t$ ,  $q \stackrel{\text{def}}{=} 2k_L x$ ,  $p \stackrel{\text{def}}{=} (2k_L / M \delta\omega) p_x$ ,  $\gamma \stackrel{\text{def}}{=} (4k_L^2 / M \delta\omega^2) V_0$ , and  $H_{\text{eff}} \stackrel{\text{def}}{=} (4k_L^2 / M \delta\omega^2) H$  then yields the dimensionless effective Hamiltonian

$$H_{\text{eff}} = \frac{p^2}{2} - \gamma(\theta + \cos \tau) \cos q. \quad (3)$$

Such a Hamiltonian describes the dynamics of a periodically driven pendulum. The associated quantum canonical commutation relation is  $[q, p] = i\hbar_{\text{eff}}$ , and we obtain  $\hbar_{\text{eff}} \hbar_{\text{eff}} = 8\omega_R / \delta\omega$ , where  $\omega_R = \hbar k_L^2 / 2M$  is the atomic recoil frequency and  $\delta\omega$  is the beating frequency between the laser waves.

Such an effective Hamiltonian clearly exhibits two of the three properties mentioned in Sec. I: the corresponding classical dynamics is governed by a single classical parameter, the dimensionless coupling strength  $\gamma$ , and is invariant under time-reversal symmetry  $(p, q, \tau) \mapsto (-p, q, -\tau)$ . It is worth mentioning that the semiclassical limit  $\hbar_{\text{eff}} \rightarrow 0$  is realized here by increasing the beating frequency  $\delta\omega$  between the two laser waves.

With our field configuration, only  $\theta \geq 1$  can be achieved. As a slight generalization, we extend the range of  $\theta$  to any positive value, since one can design other field configurations where  $\theta \leq 1$  occurs. For example,  $\theta = 0$  yields the Hamiltonian studied in Ref. [13] in a different context.

### D. Orders of magnitude

Let us give some typical experimental parameters. For rubidium atoms, the atomic parameters are  $M = 85$  amu,  $\lambda_{\text{at}} = 2\pi c / \omega_{\text{at}} = 0.78 \mu\text{m}$ ,  $\Gamma / 2\pi = 6$  MHz,  $\omega_R / 2\pi = 3.8$  kHz, and the saturation intensity  $I_{\text{sat}} = 1.6$  mW/cm<sup>2</sup>. Using far-detuned laser beams ( $2\delta_L / \Gamma = 10^4$ ) focused down to  $500 \mu\text{m}$  (power 100 mW), with a frequency difference

$\delta\omega / 2\pi = 60$  kHz, leads to  $\gamma = 0.4$  and  $\hbar_{\text{eff}} = 0.05$ . With such values, spontaneous emission can be neglected up to times of the order of few ms. It is worth noting the tiny energies which come into play ( $V_0 \sim 5$  neV), by several orders of magnitude smaller than the typical ones for mesoscopic systems.

## III. CLASSICAL DYNAMICS

### A. Poincaré surface of section

A Poincaré surface of section provides the usual tool for visualizing the classical dynamics [30]. As  $H_{\text{eff}}$  is  $2\pi$  periodic both in time and space, this surface of section simply consists in the whole phase space itself (which has the topology of a cylinder) where trajectories  $(p(\tau), q(\tau))$  are seen stroboscopically at every time period  $2\pi$ . In the following, without any substantial loss of generality, we will restrict our analysis to the case  $\theta = 1$  which is easily experimentally achieved when the standing waves have the same field strengths.

Figure 2 shows stroboscopic plots of phase space orbits for different values of  $\gamma$ . For  $\gamma = 0$ ,  $p$  is a constant of motion, so that the system is integrable and the surface of section is composed of horizontal lines. For a weak enough  $\gamma$  [Fig. 2(a)], the orbits remain confined to invariant curves. These invariant curves stratify the whole phase space, and the dynamics appears regular. One can clearly see well-separated stability islands, each being bordered by a separatrix. This is the situation encapsulated in the Kol'mogorov-Arnol'd-Moser (KAM) theorem for near-integrable motion: although no globally defined constants of motion exist, some invariant curves can still be constructed which order the dynamics. As  $\gamma$  is increased [Fig. 2(b)], more and more of the invariant curves are broken and chaotic layers start to spread around separatrices. These layers fill some portion of phase space, but the motion is still predominantly confined to invariant curves. Above some coupling threshold [Figs. 2(c)–2(e)], stochastic orbits invade the phase space, and the surviving stability islands are surrounded by a connected chaotic sea. This occurs for  $\gamma \sim 0.1$ . The phase space structure in this regime is typical of a mixed dynamics where regular orbits coexist with stochastic ones. If  $\gamma$  is increased further [Fig. 2(f)], the stability islands disappear (or are too small to be seen at this scale) and one obtains global chaos. However, we note that, even in this situation, the chaotic portion of phase space is still bounded by invariant curves, which means that chaos can only fully develop within some range of momentum  $p$ .

### B. Resonances

At this stage, let us rewrite the effective Hamiltonian as follows:

$$H_{\text{eff}} = H_0 + \gamma H_1 = \frac{p^2}{2} - \gamma \cos q - \frac{\gamma}{2} \cos(q + \tau) - \frac{\gamma}{2} \cos(q - \tau). \quad (4)$$

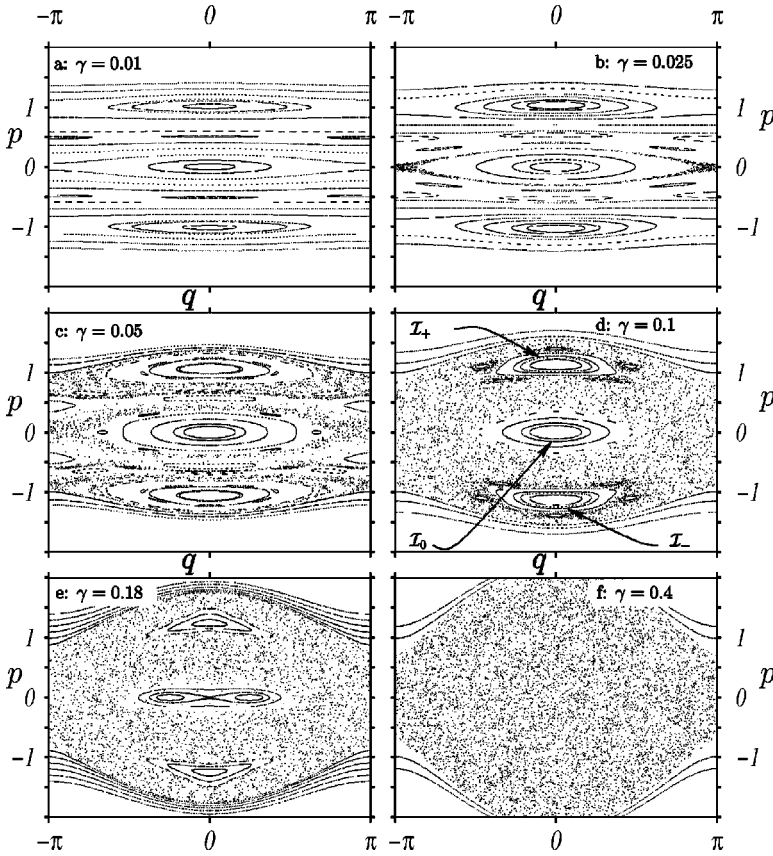


FIG. 2. Stroboscopic plots of trajectories in phase space for different initial conditions at  $\tau = 0$  and different  $\gamma$ 's. The classical dynamics is governed by Hamiltonian 3 with  $\theta = 1$ . At low  $\gamma$  values, resonance islands are visible separated by quasifree motion. As  $\gamma$  increases, the resonance islands grow and chaos appears close to the separatrices. The situation of interest for chaos-assisted tunneling is when two symmetric islands are separated by a chaotic sea, such as  $\mathcal{I}_+$  and  $\mathcal{I}_-$  in (d) and (e).

The physical interpretation of the various terms is rather simple: the two counterpropagating laser beams at frequency  $\omega_+$  create a stationary wave which, in turn, creates for the atom an effective optical potential proportional to the square of the modulus of the electric field in the standing wave; hence the  $\cos q$  dependence (it is actually  $1 + \cos q$ , but the constant term does not play any role in the dynamics). The same effective potential is due to the standing wave created by the two  $\omega_-$  counterpropagating beams. A pair of counterpropagating beams at frequencies  $\omega_+$  and  $\omega_-$  does not create a standing wave in the lab frame. However, in a frame moving at constant velocity  $v_0 = (\omega_+ - \omega_-)c/2\omega_L$ , ( $v_0 = 1$  in rescaled units) the two laser beams are shifted in frequency by the Doppler effect and appear to have equal frequency, building another stationary wave and yet another effective optical potential. In the lab frame, this appears as a modulated optical potential moving at velocity  $v_0$ . By symmetry, there are two such effective potentials moving either to the right or to the left. These are the  $\cos(q \pm \tau)$  terms in the Hamiltonian.

This form of the Hamiltonian allows us to point out the perturbative terms which may be resonant with the unperturbed frequencies. When  $\gamma = 0$ , the system is integrable since we recover free motion:  $H_{\text{eff}}$  reduces to  $H_0 = p^2/2$ , and  $(p, q)$  are exact action-angle variables. For  $\gamma > 0$ , the absence of any constant of motion generates chaos. Stroboscopic plots of phase space trajectories are no longer constrained to follow lines of constant  $H_0$ , but generically fill densely a two dimensional volume in phase space. As long as  $\gamma$  is small enough, these volumes remain thin enough not

to be distinguished from regular lines at the scale of finite precision of the measurements and/or the calculations [cf. Fig. 2(a)]. Nevertheless, for higher values of  $\gamma$ , some chaotic layers can be seen [cf. Fig. 2(b)] between regular regions. These consist of portions of phase space where trajectories are exponentially sensitive on initial conditions. From classical first-order perturbation theory (Ref. [30], Chap. 2), we can infer that a term of the form  $A \cos(sq - r\tau)$ , where  $(s, r)$  are integers, will create a resonance of width  $\Delta p = 4\sqrt{A}$  around the point  $p = r/s$ . In our case,  $s = 1$ , and there exist only three such resonances. They are located at  $p = 0$  ( $r = 0$ ) and at  $p = \pm 1$  ( $r = \pm 1$ ). This can be seen in [Figs. 2(a)–2(e)]. For each resonance there exists one stable periodic orbit and one unstable periodic orbit with periods of approximately  $2\pi|r|$ . In the stroboscopic plot of the surface of section, they appear as stable and unstable fixed points, and give rise locally to the well-known phase space portrait of a pendulum. In the following, we will denote by  $\mathcal{I}_0, \mathcal{I}_+$ , and  $\mathcal{I}_-$  the three stable islands associated with  $r = 0, +1$ , and  $-1$ , respectively. The physical interpretation of these three resonances is simple: each resonance is associated with one of the modulated potentials (either static or moving) described above. For example, the fixed point at the center of the  $\mathcal{I}_+$  resonance is associated with a periodic orbit where the atom moves at almost constant velocity  $v_0$ , being trapped in the minimum of the moving optical potential. The other two components of the potential appear along this orbit as rapidly varying potentials which are adiabatically averaged to constant values. As the atom can be trapped in any of the three modulated potentials, we obtain three stable periodic

orbits at the centers of the three resonance islands.

For a small enough  $\gamma$ , the resonances are well separated and the motion is quasi-integrable. Chaos will develop when the resonances start to overlap. This is the celebrated Chirikov's overlap criterion [31] and its evaluation gives  $\gamma \approx 0.1$  in our case. Thus chaos develops in phase space regions where the kinetic energy term and the perturbation are of the same order of magnitude. Taking into account higher perturbation orders in  $\gamma$  will shift the position in phase space of the previous resonances as well as the frequency around their stable points. For instance, it can be seen in Fig. 2(e) that the stable island  $\mathcal{I}_+$  is centered on a point having a momentum slightly larger than  $+1$ . Perturbation terms of higher order will also introduce other resonances of smaller size. It is precisely the overlap of the infinite cascade of such resonances which gives rise to the chaotic layers. Nevertheless, Chirikov's criterion already gives a good order of magnitude for the onset of chaos. For higher  $\gamma$ , the previous three resonant islands of stability have shrunk inside a large chaotic sea, and will eventually disappear completely [cf. Fig. 2(f)]. Nevertheless a revival of some stable islands can still be observed for some narrow windows of high values of  $\gamma$ . In our situation, chaos cannot invade the whole phase space, but is bounded by regular coasts. This is so because chaos develops where resonances overlap. Sufficiently far away from the resonances, atoms move so fast that they experience an average time-independent potential. Then chaos is absent and one recovers (quasi) free motion when  $|p| \gg 1$ .

### C. Typical classical phase space portrait in the chaos-assisted tunneling regime

The two resonant islands  $\mathcal{I}_\pm$ , when they exist, are related by a discrete symmetry: the time-reversal invariance. As can be seen in Fig. 3, the atoms trapped in one island cannot classically escape from it: the boundaries of the islands play the role of a dynamical barrier which atoms cannot cross. Hence jumping from one island to the other is a classically forbidden process, though it is expected to occur in quantum mechanics. This is precisely the tunneling situation we are interested in. In fact, we will study the tunneling between  $\mathcal{I}_+$  and  $\mathcal{I}_-$  for  $\gamma$  varying from 0.1 to 0.3 since, in that range, classical chaos may play a revealing role even though the two stable islands still occupy a significant volume in phase space.

Note that, in the physical situation described by  $H_{\text{eff}}$ , tunneling occurs in momentum coordinates instead of space coordinates, as usually presented in standard textbooks. The denomination of ‘‘dynamical tunneling’’ [32], refers to this situation. The reason for investigating this situation is that manipulation of cold atoms allows for a better control (preparation and detection) of momentum rather than position.

## IV. QUANTUM DYNAMICS

### A. Floquet-Bloch theory

When an autonomous Hamiltonian is spatially periodic, it is well known [33] that its spectrum is organized in energy

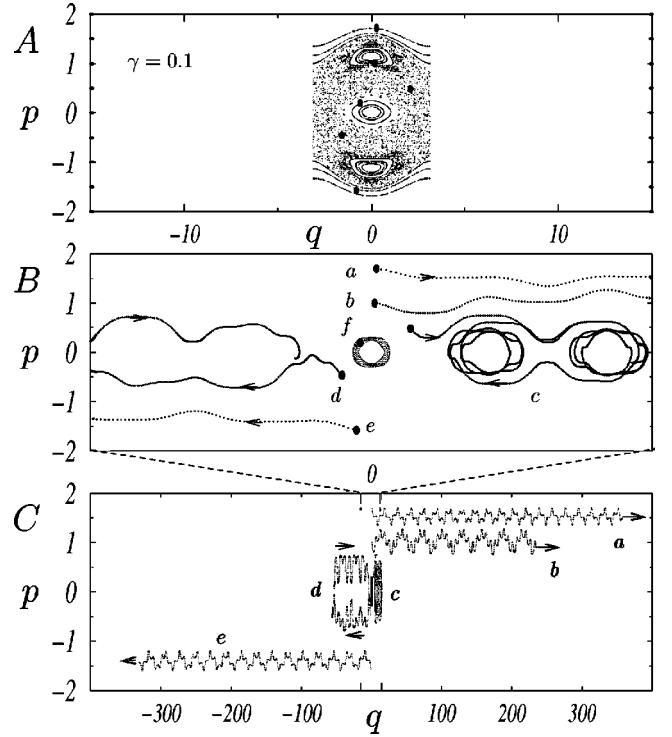


FIG. 3. Plots of some trajectories in phase space for different initial conditions ( $\gamma=0.1$ ). In A, we display a typical Poincaré surface of section as in Fig. 2, i.e., stroboscopic plots which are folded according to the spatial periodicity. The small black disks show some initial conditions. In B and C, trajectories are plotted every  $2\pi/100$  and, unlike in A, we let  $q(\tau)$  evolve continuously outside  $[-\pi, \pi]$ . Trajectories  $b$  and  $f$  are trapped in the  $\mathcal{I}_+$  and  $\mathcal{I}_0$  resonance islands, respectively. Trajectories  $a$  and  $e$  are two examples of regular quasifree motion.  $c$  and  $d$  correspond to chaotic motion; their initial conditions (at  $\tau=0$ ) lie in the chaotic sea of Fig. 2(d).

bands  $E_n(k)$ . These bands are labeled by a set of integers, the band index  $n$ , and depend continuously on a set of real numbers, the Bloch numbers  $k$ . As  $E_n(k)$  and the associated eigenfunctions are periodic functions of the  $k$ 's, all the physical information is contained in the first Brillouin zone. For 1D systems, it is simply the interval  $[-\pi/Q, \pi/Q]$ , where  $Q$  is the spatial period of the Hamiltonian.

When the Hamiltonian is time periodic, with a period  $T$ , the analog of the Bloch theory is the Floquet theory [34–36]. The eigenvalues of the evolution operator  $U(\tau+T, \tau)$  over one period take the form  $e^{-i\epsilon T/\hbar_{\text{eff}}}$ . The  $\epsilon$ 's are  $\tau$ -independent real quantities which are called the quasienergies of the system. Due to the time periodicity, the quasienergy spectrum as well as the associated eigenfunctions are now invariant under  $\epsilon \mapsto \epsilon + 2\pi\hbar_{\text{eff}}/T$ .

For  $H_{\text{eff}}$ , the application of Bloch and Floquet theorems with  $Q=T=2\pi$  yields a spectrum made out of quasienergy bands  $\epsilon_n(k)$ , where  $n$  goes over the whole set of integers (for a detailed derivation, see Appendix B). For brevity, we will define  $|n, k, \tau\rangle$ , the ket at time  $\tau$  with Bloch angle  $k$ , with quasienergy  $\epsilon_n(k)$ , which is a solution of the Schrodinger equation [following the notations of Appendix B, we have set  $|n, k, \tau\rangle \stackrel{\text{def}}{=} |\psi_{\epsilon_n(k), k}(\tau)\rangle$ ]. We will also define  $|n, k\rangle$

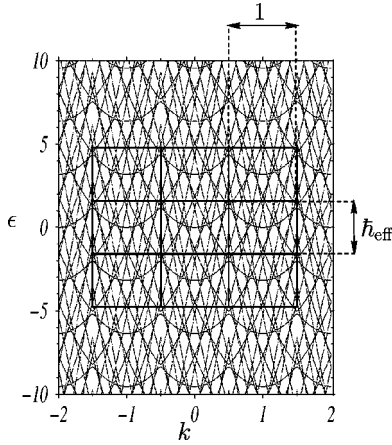


FIG. 4. For a Hamiltonian that is  $Q$  periodic in space and  $T$  periodic in time, the quasienergy spectrum is made of bands that are  $2\pi/Q$  periodic in the Bloch numbers and  $2\pi\hbar_{\text{eff}}/T$  periodic in quasienergies. Such a spectrum is shown here for Hamiltonian 3 ( $Q=2\pi$ ,  $T=2\pi$ ), with  $\gamma=0.18$  and  $\hbar_{\text{eff}}=3.1787$ .

$\stackrel{\text{def}}{=} |n, k, \tau=0\rangle$ . As it can be seen in Fig. 4, the band spectrum has the topology of a torus since it is both periodic in quasienergy (with period  $\hbar_{\text{eff}}$ ) and Bloch number (with period 1).

### B. Numerical calculation of the Floquet eigenstates

As derived in Appendix B, the Floquet eigenstates can be obtained by a diagonalization of the Floquet-Bloch operator  $\tilde{K}$ ,

$$\tilde{K}(\hat{p}, \hat{q}, \tau, k) = \frac{(\hat{p} + \hbar_{\text{eff}}k)^2}{2} - \gamma \cos \hat{q}(1 + \cos \tau) - i\hbar_{\text{eff}} \frac{d}{d\tau}, \quad (5)$$

with periodic boundary conditions in both time and space. The eigenvalues, which depend on the Bloch vector  $k$ , are the quasienergies of the system. The band spectrum is symmetric with respect to the axis  $k=0$ , since operator 5 is invariant under the transformations  $k \mapsto -k$  and  $p \mapsto -p$ . From the expression of the Floquet-Bloch operator and the boundary conditions, it is very natural to expand the eigenstates on a basis set composed of products of the type  $\phi_{lm}(\tau, q) = \exp(in\tau)\exp(imq)$ , which automatically obey the periodic boundary conditions. In such a basis, the operator  $\tilde{K}$  has very strong selection rules, namely,

$$|\Delta n| \leq 1 \quad \text{and} \quad |\Delta m| \leq 1 \quad (6)$$

All matrix elements violating one of these selection rules is zero. Hence the matrix representing the operator  $\tilde{K}$  in this basis is sparse and banded, and all matrix elements have simple analytical expressions. This is well suited for numerical diagonalization (powerful algorithms exist, for example the Lanczos algorithm). All the numerical results presented here use this method. We checked that the effect of the truncation of the basis is negligible: the size of the Floquet ma-

trix is considered to be sufficiently large when increasing it modifies the value of the quasienergy on the scale of the numerical noise only, say  $10^{-15}$  in double precision. Not only is this criterion a proof of the algorithmical convergence, but it also is a safeguard against numerical discrepancies, since we are looking for exponentially small quantities.

### C. Husimi representation and classification of the quantum states

Classical dynamics is very illuminating when describing the states  $|n, k, \tau\rangle$ . In order to strengthen the correspondence between classical phase-space structures and quantum states, it is convenient to work with the Husimi representation of quantum states [37].

Such a representation associates, with each quantum state  $|\psi\rangle$ , a phase space function  $\psi^{\text{H}}(p, q)$  (where  $p$  and  $q$  are real numbers) defined by

$$\psi^{\text{H}}(p, q) \stackrel{\text{def}}{=} N_{\psi} |\langle z | \psi \rangle|^2, \quad (7)$$

where  $|z\rangle$  is the normalized coherent state corresponding to the complex number  $z = (q + ip)/\sqrt{2\hbar_{\text{eff}}}$ .  $N_{\psi}$  is a  $(p, q)$ -independent normalization factor. Because  $|z\rangle$  is a minimal Gaussian wave packet with average momentum  $p$  and average position  $q$ , the Husimi function  $\psi^{\text{H}}(p, q)$  contains some information about the degree of localization of  $|\psi\rangle$  in phase space.

The minimal cell size in phase space, allowed by the Heisenberg inequalities, is  $\hbar_{\text{eff}}$ . Let us see how classical phase space structures of a typical size larger than  $\hbar_{\text{eff}}$  are mirrored at the quantum level. In Figs. 5 and 6 we plot some values of  $\epsilon_n(k)$  corresponding to Hamiltonian 3 for specified fixed values of  $\gamma$  and  $\hbar_{\text{eff}}$ . von Neumann–Wigner arguments [38] claimed that, generically, no exact degeneracy can occur: rather one obtains avoided crossings. Of course, this is relevant provided the minimal energy splitting is greater than the resolution in energy. Some Husimi functions are plotted in Figs. 5 and 6 [(a)–(f)].<sup>1</sup>

In Appendix B, it is shown that we have

$$v_{n,k} \stackrel{\text{def}}{=} \frac{1}{T} \int_0^T \langle n, k, \tau | \hat{p} | n, k, \tau \rangle d\tau = \frac{1}{\hbar_{\text{eff}}} \frac{\partial \epsilon_n}{\partial k}, \quad (8)$$

$$|z, k\rangle \stackrel{\text{def}}{=} \sum_{m \in \mathbf{Z}} e^{imkQ} |z + mQ\rangle, \quad (9)$$

and define, for instance,

<sup>1</sup>A technicality should be mentioned here:  $|u_{\epsilon,k}\rangle$  and  $|\psi_{\epsilon,k}\rangle$  obey some spatial boundary conditions which are lost when working with their Husimi representations, essentially because the coherent states do not fulfill these properties themselves. To deal with spatially (quasi)periodic phase space functions, it is necessary to unfold the coherent states [39] into

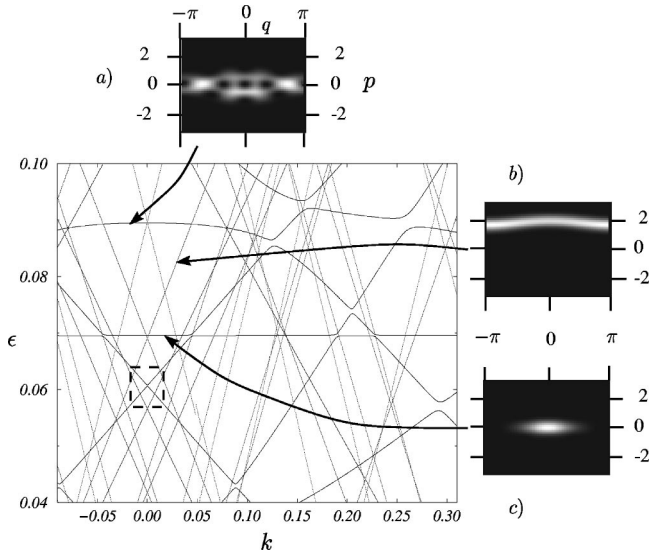


FIG. 5. Quasienergy bands for  $\gamma=0.18$  and  $\hbar_{\text{eff}}=0.2037$  and some Husimi representations of typical states. In (b) we show a quasifree state with a well defined average velocity (the derivative of the energy level with respect to  $k$ ) localized in phase space on regular trajectories [compare with Fig. 2(e)]. On this scale, the avoided crossings with other bands cannot be resolved. In (c) we show a state localized in the central stable island  $\mathcal{I}_0$  (actually the ‘‘ground state’’). Far from quasidegeneracies the average velocity of this state is zero. In (a) we give an example of a chaotic state, whose Husimi function is localized in the chaotic sea [compare with Fig. 2(e)]. Unlike the former states, the average velocity fluctuates when the Bloch angle  $k$  is varied. The band spectrum is symmetric with respect to the axis  $k=0$ , since operator  $\mathcal{H}$  is invariant under the transformations  $k \mapsto -k$  and  $\hat{p} \mapsto -\hat{p}$ . The tunneling situation due to the time-reversal symmetry corresponds to the dashed squared zone (around  $k=0$ ), which is enlarged in Fig. 6.

$$\psi_{n,k}^{\text{H}}(p,q,\tau) \stackrel{\text{def}}{=} N |\langle z,k | \psi_{n,k}(\tau) \rangle|^2. \quad (10)$$

which generalizes the velocity theorem (Ref. [33], Appendix E) to periodic time-dependent Hamiltonians.

Figure 5(b) shows an example of the Husimi representation of a state with sufficiently high average velocity to be like a free eigenstate of  $H_0$ . Far from quasidegeneracies it is localized in a narrow strip of width  $\Delta p \sim 2\pi\hbar_{\text{eff}}/\Delta q \sim \hbar_{\text{eff}}$  (since  $\Delta q$  covers  $2\pi$ ), and which is centered on one of the two classical phase space trajectories of energy about  $v_{n,k}^2/2$  [compare with Fig. 2(e)]. Its quasienergy band (Fig. 5) is an arc of the parabola of the free motion, but can hardly be distinguished from a straight line of slope  $v_{n,k}$  if  $k$  is restricted to one Brillouin zone. We will naturally call these states quasifree states.

Some states have their Husimi functions localized in the resonant stable islands (in  $\mathcal{I}_0$  but also in  $\mathcal{I}_{\pm}$ ). The number of these states is semiclassically given by the volume of these islands divided by  $2\pi\hbar_{\text{eff}}$ . Far away from quasidegeneracies, these states are at any time centered on the stable periodic orbit: this can be explained within a semiclassical approach, and can be observed in Fig. 5(c) for a state localized in  $\mathcal{I}_0$ , and in Figs. 6(d) and 6(e) for states in  $\mathcal{I}_-$  and  $\mathcal{I}_+$

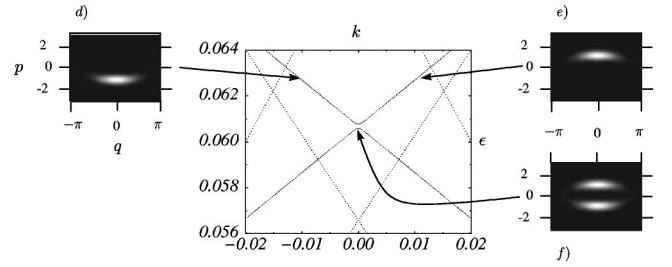


FIG. 6. Quasienergy bands for  $\gamma=0.18$  and  $\hbar_{\text{eff}}=0.2037$  and some Husimi representations of typical states. This is a zoom of the dashed squared zone in Fig. 5. For  $k \neq 0$ , one can find states like those in (d) or (e), whose Husimi function is localized in one stable island  $\mathcal{I}_-$  or  $\mathcal{I}_+$  [compare with Fig. 2(e)]. In the frame, where the center of the island is fixed, these states correspond to the ‘‘ground’’ states (some excited states may of course exist if  $\hbar_{\text{eff}}$  is small enough, as can be seen in Figs. 12 and 13). For  $k=0$ , we recover time reversal symmetry through the existence of quasidegenerate doublets of symmetric or antisymmetric combinations. This is a typical tunneling situation: following the state in (e) (which has an average velocity about  $+1$ ) adiabatically with  $k$ , by decreasing  $k$  we obtain a state in (d) that has a reversed velocity. This reversal of the velocity is a classically forbidden process (compare with orbit  $b$  in Fig. 3).

respectively. Their average velocity as well as their Husimi functions depend exponentially weakly on the Bloch parameter  $k$ .

The last class of states which can be encountered corresponds to chaotic ones, i.e., states whose Husimi functions are negligible on a typical distance of  $\sqrt{\hbar_{\text{eff}}}$  out of the chaotic seas [cf. Fig. 5(a)]. Unlike the previous ones, their Husimi functions are very sensitive to any variation of  $k$  since they are delocalized in the whole chaotic sea which spreads over all elementary cells. The large classical distribution of possible velocities is to be linked to the very fluctuating slopes of the quasienergies as  $k$  is varied.

#### D. Tunneling states

Although the system as a whole is of course time-reversal invariant, this is no longer true for its restriction at a fixed value  $k$  of the Bloch vector. Indeed, the operator  $\tilde{K}$  is not time reversal invariant, because of the crossed term  $k\hat{p}$ . In other words, the time-reversed partner of a state with a Bloch vector  $k$  is a state with a Bloch vector  $-k$ . It is only at the special value  $k=0$  (and also  $k=1/2$  since  $k$  is defined modulo 1) that  $\tilde{K}$  is invariant under time-reversal symmetry. Therefore, it corresponds to the typical situation of tunneling between  $\mathcal{I}_+$  and  $\mathcal{I}_-$ . Every state localized in an island around  $|p|=1$  is quasidegenerate with another one. These doublets represent a symmetric and antisymmetric combination of states localized in one island only [cf. Fig. 6(f)]. The energy splitting  $\Delta\epsilon_n$  of these states for  $k=0$  is precisely the signature of tunneling: it is  $\pi\hbar_{\text{eff}}$  divided by the typical time an atom takes to oscillate from one island to its time-reversed image, i.e., to reverse the sign of its velocity.

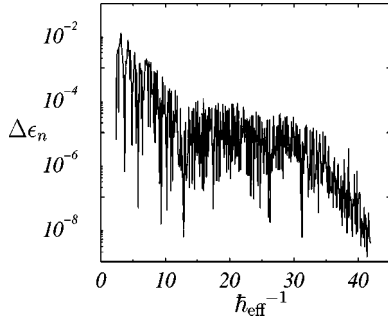


FIG. 7. Fluctuations of the energy splittings  $\Delta\epsilon_n$  between pairs of symmetric or antisymmetric states localized in the  $\mathcal{I}_\pm$  resonance islands (here shown for the “ground state” inside the island). The classical dynamics is fixed at  $\gamma=0.18$  [compare with Fig. 2(e)]. The existence of large fluctuations over several orders of magnitude is a signature of chaos-assisted tunneling. On the average,  $\ln|\Delta\epsilon_n|$  appears to decrease more or less linearly with  $\hbar_{\text{eff}}^{-1}$  except for the plateau at  $15 \leq \hbar_{\text{eff}}^{-1} \leq 30$ .

## V. CHAOS-ASSISTED TUNNELING

### A. Large fluctuations

After having selected the two quasienergy bands corresponding to the two states which are localized most deeply inside the islands  $\mathcal{I}_\pm$ , we are able to plot the splitting as a function of  $\hbar_{\text{eff}}$ . The great advantage of studying fluctuations when the effective Planck constant is varied is that it does not affect the classical dynamics. The behavior of the splitting is very different whether chaos is present at the  $\hbar_{\text{eff}}$  scale or not. In the chaotic regime (cf. Figs. 7 and 8), that is when  $\hbar_{\text{eff}}$  varies in a range where chaotic seas can be resolved, the splittings vary rapidly versus the change of any parameter, in our case  $\hbar_{\text{eff}}$ . Moreover, the variations of the splittings, despite being perfectly deterministic, are apparently erratic—without any regular structure—and cover several orders of magnitude. They show that direct coupling to the chaotic sea is the key mechanism for their understanding, and are a signature of chaos-assisted tunneling [40,41]. In fact these huge fluctuations are reminiscent of the universal

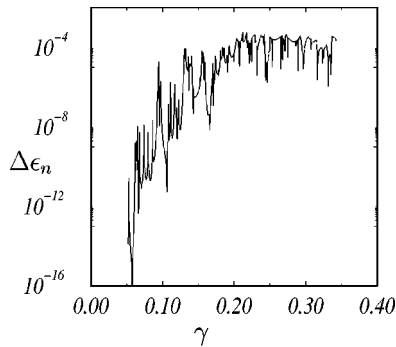


FIG. 8. Fluctuations of the energy splittings  $\Delta\epsilon_n$  between the pair of symmetric or antisymmetric states ( $\hbar_{\text{eff}}^{-1}$  is fixed at 19.309) as a function of  $\gamma$ . Again, large fluctuations over several orders of magnitude are a signature of chaos-assisted tunneling. The global increase with  $\gamma$  is due to the growth of the chaotic sea as  $\gamma$  increases; see Fig. 2.

conductance fluctuations observed in mesoscopic systems [42,43] since tunneling is nothing other than wave transport from one stability island to the other. In contrast, in the regular regime where chaotic seas are smaller than  $\hbar_{\text{eff}}$ , the splittings are expected to vary smoothly [6].

In Fig. 7, we show the splittings of the pair of states localized at the center of the resonance islands  $\mathcal{I}_\pm$ , as a function of  $\hbar_{\text{eff}}$ . They display huge fluctuations over about four orders of magnitude while the general trend is a decrease as  $\hbar_{\text{eff}} \rightarrow 0$ . Similarly, when plotted as a function of  $\gamma$  (see Fig. 8), they also display large fluctuations. The general trend here is a fast increase of the typical splitting with  $\gamma$ ; this is associated with a shrinking of the regular island when  $\gamma$  increases, which results in an increasingly large tunneling probability. The overlap of the regular states (still supported by the islands) with the chaotic states increases. Therefore, the coupling between the two components of the tunneling doublets which involves the chaotic states increases as well. In order to understand both the general trend and the origin of the fluctuations, two points of view can be used: a quantum point of view and a semiclassical one.

### B. Semiclassical interpretation

If the chaotic sea is large, it is rather intuitive that it can be easier first to tunnel from the center of the regular island to the chaotic sea, then propagate freely in the chaotic sea to the vicinity of the symmetric island, and finally tunnel to the center of the symmetric island than directly tunneling between the two islands. Actually, a rigorous quantitative treatment of this problem is highly nontrivial, and is beyond the scope of this paper. The crucial point is that because the chaotic sea is explored rapidly and densely, it does not cost anything to cross the chaotic sea. Tunneling trajectories can be viewed as complex trajectories (i.e., with complex position and momentum) connecting the symmetric islands. The tunneling amplitude associated with a single tunneling orbit is essentially  $\exp[-\text{Im}(S)/\hbar_{\text{eff}}]$ , where  $S$  is the complex action of the tunneling orbit. In a typical one-dimensional system (like a double well), there is only one such trajectory at each energy, and the tunneling rate thus displays the well-known exponential decrease. In a chaotic system, it may happen that there is a whole set of tunneling trajectories whose imaginary parts of the action are essentially identical. In such conditions, the actual tunneling amplitude is the sum of all individual amplitudes (each taken with its proper phase) which results in a very complicated quantity which fluctuates when parameters are changed. In some sense, this is analogous to the speckle pattern obtained when plenty of optical rays with various geometries are randomly interfering. This is the very origin of the (deterministic) fluctuations of the tunneling rates, and consequently of the energy splittings. The general trend (exponential decrease) is related to the typical imaginary part of the action of the tunneling trajectories.

### C. Quantum point of view

A complementary quantum point of view is possible. One can divide the eigenstates of the system into two subsets:

“regular” states localized in the resonance islands, and “chaotic” states localized in the chaotic sea. The two sets are only weakly coupled by tunneling. Because there are two symmetric islands, the regular states are essentially doubly degenerate (neglecting *direct* tunneling). The chaotic sea also has twofold symmetry, and states can be classified as even or odd. The two series of odd and even states ignore each other. Hence, when by accident, an even chaotic state is almost degenerate with an even regular state, they repel each other: at the same time, there is usually no odd chaotic state with the same energy. Thus the odd regular state is not significantly repelled. Hence the splitting appears due to different shifts of the even and odd regular states. Close to any avoided crossing between either the odd or even regular state and a corresponding chaotic state, a large splitting is obtained. Conversely, far from any avoided crossing, the splitting is small. Hence the fluctuations are associated with the existence of a large number of successive avoided crossings. The typical size of these fluctuations is related to the typical size of the avoided crossings, while the typical parameter range of these fluctuations is the distance (in parameter space) between two consecutive avoided crossings. A model implementing this idea (each regular state is independently and randomly coupled to the chaotic states of the same symmetry) was proposed in Ref. [44] and further used in Ref. [45]. In this model, the chaotic states are modeled by a Hamiltonian belonging to the Gaussian orthogonal ensemble of random matrices while the coupling between the regular state and the chaotic state is also taken as a random Gaussian variable. With these assumptions, the splitting distribution can be calculated. Let us denote the mean level spacing between chaotic states by  $\Delta$ , and the typical strength of the coupling between the regular states and the chaotic sea by  $\sigma$ . Only if  $\sigma \ll \Delta$  is a regular state weakly coupled to the continuum (if this inequality is violated, the regular state is completely diluted in the chaotic sea by the strength of the coupling). We thus assume the inequality to be valid. Then, the distribution of splittings  $\Delta\epsilon$  is given by

$$P(\Delta\epsilon) = \frac{1}{\pi} \frac{s}{s^2 + \Delta\epsilon^2} \quad \text{for } |\Delta\epsilon| < \sigma, \\ P(\Delta\epsilon) \approx 0, \quad \text{for } |\Delta\epsilon| > \sigma, \quad (11)$$

where

$$s = \frac{\sqrt{2}\pi\sigma^2}{\Delta}. \quad (12)$$

The interpretation is rather simple. The maximum splitting is observed exactly at the avoided crossing where the levels are shifted by  $\pm\sigma/2$  on both sides of their unperturbed positions. Hence the splitting cannot be larger than about  $\sigma$ . In fact, there is an exponentially decreasing tail in the distribution  $P(\Delta\epsilon)$  (associated with the Gaussian fluctuations of  $\sigma$ ) which we do not detail here because it is not relevant in our present case.  $s$  is the typical splitting one expects to observe: it corresponds to a shift typically due to the closest chaotic state. The full distribution is a (truncated) Cauchy distribu-

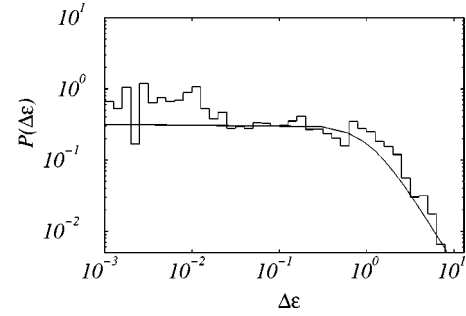


FIG. 9. Statistical distribution of the energy splittings  $\Delta\epsilon$  (normalized to the typical splitting) between pairs of symmetric or antisymmetric states localized inside the  $\mathcal{I}_{\pm}$  resonance islands ( $\gamma = 0.18$ ,  $k=0$ ), represented on a double logarithmic scale. One can clearly distinguish two regimes: constant at small  $\Delta\epsilon$  followed by a  $1/\Delta\epsilon^2$  decrease, and finally a rapid cutoff (not shown in the figure). The solid line is the Cauchy distribution predicted by random matrix theory.

tion: it is obtained as the overall effect of all chaotic states lying above or below in energy. Note that, in the absence of a truncation of the Cauchy distribution, the average splitting is not defined because the corresponding integral diverges. Hence it is better to discuss the typical splitting  $s$  rather than the average splitting. It is the slow decrease of the Cauchy distribution for large splitting that is responsible for the huge fluctuations in the splittings, which can be as large as  $\sigma \gg s$ . This is reminiscent of random processes such as Lévy flights where rare events are dominant [46].

In Fig. 9, we show the statistical distribution of splittings that we obtain numerically in the chaotic regime (normalized to the typical splitting in order to work with  $s=1$ ). The distribution is shown on a double logarithmic scale, and compared with the Cauchy distribution. One can clearly see two regimes: for small  $|\Delta\epsilon|$ ,  $P(|\Delta\epsilon|)$  is almost constant and decreases with a slope -2 for large  $|\Delta\epsilon|$ . The agreement with the Cauchy distribution is very good, which proves that the model catches the essential part of the physics in this system.

The typical splitting  $s$  is proportional to the square of the tunnelling matrix element from the initial state to the chaotic sea. Hence it is expected to decrease roughly as  $\exp[-2 \text{Im}(S)/\hbar_{\text{eff}}]$ , where  $S$  is the complex action of tunneling orbits (the mean level spacing scales as a power of  $\hbar_{\text{eff}}$ , and is thus a correction to the main exponential decrease). This is roughly what is observed in Fig. 7. Note, however, that there is a plateau in the range  $15 \leq \hbar_{\text{eff}}^{-1} \leq 30$ . A similar observation was made in Ref. [47], Fig. 3. Although this is not a crucial problem (the statistics of the splitting distribution is not affected), a detailed explanation of this behavior is still lacking (however, see Ref. [47]). Finally, it should be interesting to calculate explicitly some of the complex tunneling orbits in our specific system in order to compare the imaginary part of their actions with the slope in Fig. 7. This work is currently in progress.

## VI. EXPERIMENTAL SIGNAL

As can be seen in Fig. 5, the splittings we want to measure correspond to very tiny scales among the other struc-

tures in the band spectrum. For  $\hbar_{\text{eff}} \approx 0.1$  e.g., the tunneling times are about  $\hbar_{\text{eff}}/\Delta\epsilon \sim 10^3$  times the typical period ( $T$  on the order of a few  $\mu\text{s}$ ). The observation of atoms having reversed their velocity is therefore still possible since, for 1 ms, spontaneous emission has not begun to spoil our dynamical model. Nevertheless, measuring tiny splittings which are hidden so deeply in the spectrum is far from being straightforward. Several steps are needed: preparation of the initial state, the experiment itself (where chaos-assisted tunneling takes place), and an analysis of the final state. During the first step, one must prepare a state localized inside one resonance island, i.e., localized both in position and momentum spaces. The idea is to use an adiabatic transfer from an initial state extended in position space by slowly branching the effective potential. Although the second step looks trivial (one just has to wait), the dispersion in the vector angle  $k$  makes things much more difficult as only the  $k=0$  states are related by time-reversal symmetry (see Sec. IV D), and thus tunnel relatively fast. However, it is possible to overcome this difficulty, as explained below. Finally, the detection should be rather easy, using velocity dependent Raman transitions. We now explain in detail how the various steps can be worked out.

#### A. Adiabatic preparation of the atoms in one lateral stable island

The first step consists of preparing an initial cloud of cold rubidium atoms in order to have it located in one of the stable island, e.g.,  $\mathcal{I}_+$ , only. Using a standard magneto-optical trap, one can obtain a more or less thermal distribution of atoms with a velocity on the order of a few times the recoil velocity  $v_{\text{rec}} = \hbar k_L/M = 6$  mm/s. However—as shown below—this is probably too much for a good measurement of the tunneling splitting. Additional techniques (side-band cooling [48], Raman cooling [49,50]) make it possible to obtain a subrecoil velocity distribution, i.e., atoms with an average momentum  $p_0$  and a thermal dispersion  $\Delta p_x = M\Delta v = M\alpha v_{\text{rec}}$  with  $\alpha$  significantly smaller than 1. We chose the initial momentum to be  $M\delta\omega/2k_L$ , so that, on average, the atoms exactly follow one of the sliding standing wave created by a pair  $\omega_{\pm}$  of laser beams.

The next step is to slowly (i.e., adiabatically) switch on the standing waves. During this phase, the spatial periodicity is preserved, and the Bloch vector  $k$  is thus a conserved quantity. Initially, the momentum  $p_x$  is nothing but the Bloch vector (modulo a integer multiple of the recoil momentum). Thus, by preparing a subrecoil initial state, one populates only a small range of  $k$  values and, for each  $k$  value populated, a single state (momentum eigenstate). In other words, the initial momentum distribution becomes a statistical mixture of Bloch states with  $\Delta k = \alpha/2$  in a single energy band. More generally, if the initial momentum distribution is not a subrecoil one, but has a width equal to  $\alpha$  recoil momenta (with  $\alpha > 1$ ), about  $\alpha$  bands will be populated.

Switching on the standing waves increases the optical potential  $V_0$  and therefore  $\gamma$  from zero and enlarges the resonance islands. In the frame moving with velocity  $p_0/M = \delta\omega/2k_L$ , the atoms “feel” a pendulumlike potential

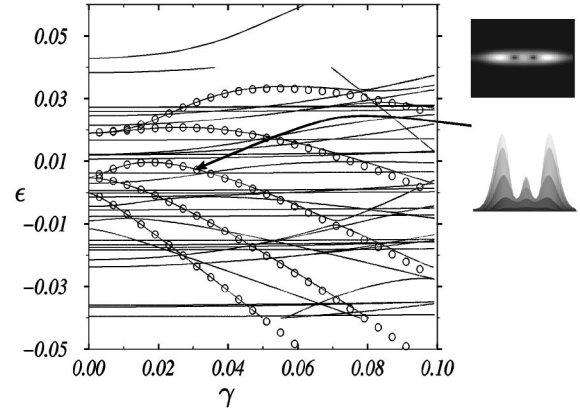


FIG. 10. Comparison between the quasienergies of Hamiltonian 3 (lines) and the energies (circles) obtained from the pendulum approximation in the stable island  $\mathcal{I}_0$  ( $\hbar=0.0976$ ,  $k=0$ ). The avoided crossings that appear at  $\gamma \sim 0.07$  illustrate the influence of classical narrow chaotic seas on the quantum properties. The Husimi distribution of the second excited state localized in  $\mathcal{I}_0$  for  $\gamma = 0.03$  is shown.

$-\frac{1}{2}\gamma \cos q$  (in scaled coordinates) in addition to some rapidly time varying terms. Consequently, they will adiabatically localize in the potential minima, that is at the center of the resonance island. Increasing  $\gamma$  successively localizes an increasing number of states in  $\mathcal{I}_+$ . The switching time must be sufficiently long as compared to the beating period (in this case the discarded terms are still rapidly oscillating) but also to the inverse of the minimum energy gap (of the order of  $\hbar_{\text{eff}}^{-1}$  if  $\Delta k$  is sufficiently narrow). In order to trap all the initially populated states,  $\gamma$  has to be sufficiently large. For a given Bloch angle, we want to localize the  $\alpha$  first states. The quantum energies of a pendulum are given by the eigenvalues of the Mathieu equation (Ref. [51], Chap. 20) (see Figs. 10 and 11). For a pendulum whose Hamiltonian is

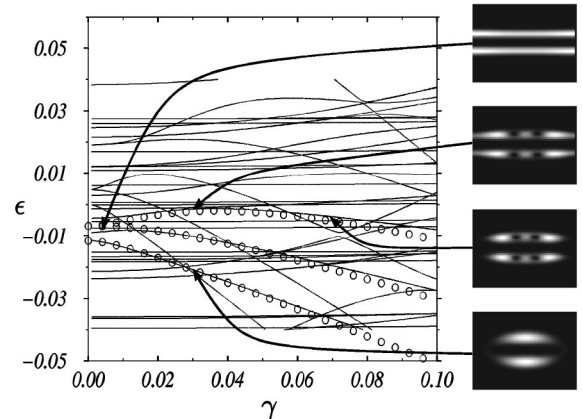


FIG. 11. Comparison between the quasienergies of Hamiltonian 3 (lines) and the energies (circles) obtained from the pendulum approximation in the stable islands  $\mathcal{I}_{\pm}$  ( $\hbar=0.0976$ ,  $k=0$ ). The three upper Husimi plots show how a quasifree state doublet becomes progressively localized in a stable island when  $\gamma$  increases. The lower Husimi plot corresponds to the “ground” state of the pendulum approximation in the stable islands  $\mathcal{I}_{\pm}$  for  $\gamma=0.03$ .

$$H_{\text{pend}} = \frac{p^2}{2} - \frac{\gamma}{2} \cos q, \quad (13)$$

the phase space volume enclosed by the separatrix is  $16\sqrt{\gamma/2}$ . Semiclassically, this corresponds to  $16\sqrt{\gamma/2}/(2\pi\hbar_{\text{eff}})$  states. This number will be of the order of  $\alpha$  when  $\gamma$  reaches the value

$$\gamma_{\text{adiab}} \approx \frac{(\alpha\pi\hbar_{\text{eff}})^2}{128}. \quad (14)$$

Figures 10 and 11 show the exact energy levels of the system together with the ones using the pendulum approximation and the Mathieu equation, as well as plots of selected Husimi representations for few eigenstates. This allows us to check the following.

(i) The pendulum approximation works well in the regime of interest, up to about  $\gamma=0.1$ .

(ii) The semiclassical estimate of the number of trapped states is sufficiently accurate for our purpose.

(iii) The Husimi representations of the trapped states are well-localized: especially, the states in Fig. 11 have two well-separated components in the  $\mathcal{I}_+$  and  $\mathcal{I}_-$  islands, meaning that we are in a real case of tunneling.

(iv) During the initial increase of  $\gamma$ , the ‘‘ground’’ state is well isolated (in energy) from the other ones, which means that an adiabatic preparation is possible.

Nevertheless, for this adiabatic preparation to be valid, we must make sure that  $\gamma$  has not reached a range where chaos has non-negligible effects on quantum properties. Physically, we want chaotic layers at  $\gamma = \gamma_{\text{adiab}}$  to have a small volume compared to the Planck constant. From Fig. 10, we can obtain the upper bound limit of  $\gamma$  by estimating when the (small) avoided crossings become too large to be passed diabatically. For  $1/50 < \hbar_{\text{eff}} < 1/5$ , we observe that chaos has no influence for  $\gamma < \gamma_{\text{chaos}} \approx 0.04$ .

The adiabatic preparation of all the atoms in one stable island will be achieved if  $\gamma_{\text{adiab}} < \gamma_{\text{chaos}}$ , that is, if the atoms are cold enough to have

$$\alpha < \frac{8\sqrt{2\gamma_{\text{chaos}}}}{\pi\hbar_{\text{eff}}} \approx \frac{0.7}{\hbar_{\text{eff}}}. \quad (15)$$

In every situation considered in the following, we will have to check that this condition is fulfilled. Next we have to reach the desired value for  $\gamma$  ( $\approx 0.18$ ) in the chaotic regime while preserving the state in the island. This will be achieved if  $\gamma$  is increased sufficiently fast so that all encountered avoided crossings with chaotic states are passed diabatically. Hence the whole preparation of the initial atomic state proceeds by two steps: a first adiabatic increase of  $\gamma$  at the very beginning to significantly populate regular states in one island, followed by a diabatic increase of  $\gamma$  to preserve them in the chaotic regime.

### B. How to force tunneling?

As discussed in Sec. IV D, the tunneling splitting is small only for a Bloch vector  $k=0$ . As it is not presently possible

to prepare only this value of  $k$  in a real experiment, it seems at first sight that only a small fraction of atoms (close to  $k=0$ ) may effectively tunnel, hence considerably reducing the signal to noise ratio. A solution is to force all atoms to go through the  $k \approx 0$  region. The simplest idea is to impose a slow increase of the  $k$  value, by adding a constant external force  $F$  from outside. Then the full Hamiltonian that governs the dynamics is

$$H'(p, q, \tau) = H(p, q, \tau) - qF. \quad (16)$$

The potential  $V$  induces a dynamical drift in the Bloch angle:

$$\frac{d}{d\tau} k(\tau) = \frac{1}{\hbar_{\text{eff}}} F. \quad (17)$$

It is shown in Appendix C that this relation, which is well known in the time independent case (see, for instance, Ref. [52], Chap.6), remains valid when  $H$  is periodic in time.

A convenient way of realizing experimentally such a constant force is to chirp the laser frequencies, that is make all the frequencies drift linearly in time. In an accelerated frame, the laser frequencies appear as constants, and we are back to our model. However, in this noninertial frame, the constant acceleration is translated in a constant force; hence the system is governed by Eq. (16). This method has been used with cold atoms (see Ref. [24]).

The global result is a slow drift of the  $k$  distribution. This causes the various  $k$  classes to come successively closer to  $k=0$ , and thus become able to tunnel. Whether the atom will effectively tunnel or not depends on the time scale on which  $k$  changes. If  $k$  varies rapidly, the avoided crossing at  $k=0$  is crossed diabatically, i.e., the velocity distribution will not be modified. If  $k$  varies slowly, it is crossed adiabatically (rapid adiabatic passage). The Landau-Zener formula [53] yields a typical time scale for the crossover between diabatic and adiabatic crossing.

Figures 12 and 13 illustrate, for  $\hbar_{\text{eff}}=0.2037$ , the drift of atoms initially localized in  $\mathcal{I}_+$  (one energy band) whose distribution in  $k$  covers  $1/10$  of the Brillouin zone from  $k \approx -1/10$  to  $k \approx 0$  (a subrecoil initial velocity distribution with a width on the order of  $v_{\text{rec}}/5$ ). We allow the atoms to evolve under the force  $F$  in order to obtain a global translation of  $1/10$  in  $k$ . After moving across the splitting at  $k=0$ , if the force  $F$  is weak to follow the energy level adiabatically, the average momentum of the atoms has reversed its sign, as can be seen in Fig. 13. Measuring the critical value of  $F$  for this Landau-Zener-like transition furnishes a means to measure the splitting. Another possibility would be to modulate the external force (and thus the  $k$  values) periodically in time in order to induce a resonant transfer between  $\mathcal{I}_+$  and  $\mathcal{I}_-$ .

In any case, the method may work only if no other avoided crossing come into play. Numerical investigations show that there are mainly tiny avoided crossings along the energy curve of interest. However, as a general rule, there are usually a few avoided crossings with similar or larger sizes than the avoided crossing of interest. If such an avoided crossing is also passed adiabatically, it will of course spoil the momentum distribution. Hence it is crucial for the initial

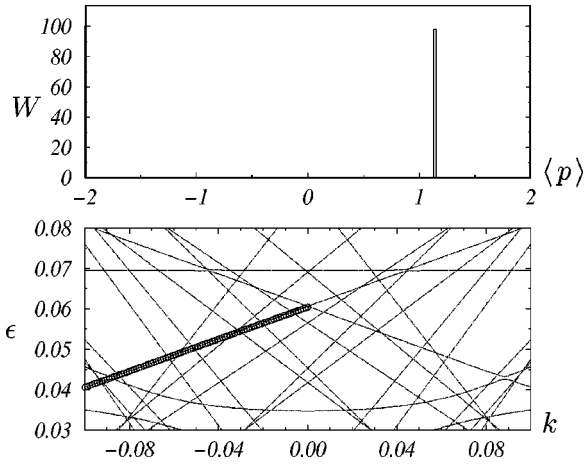


FIG. 12. In order to measure the tunneling splitting at  $k=0$  (see Figs. 5 and 6), the atoms are prepared into states localized inside the  $\mathcal{I}_+$  resonance island. The average momentum distribution (top graph) is peaked at a value slightly larger than +1 in agreement with Fig. 2. The initial states occupy one-tenth of the first Brillouin zone, and are represented by the circles in the lower graph. ( $\hbar_{\text{eff}} = 0.2037$ ,  $\gamma = 0.18$ .) After an adiabatic sliding of  $\Delta k \approx 0.1$ , the states are populated, and the average momentum distribution is shown in Fig. 13.

$k$  distribution to be sufficiently narrow to avoid this problem. Hence a subrecoil velocity distribution seems necessary.

### C. Detection

After the atoms have interacted with the modulated waves, one can switch off the lasers either abruptly or adiabatically (in which case the atoms adiabatically leave the resonance island). In both cases, the atoms which have tun-

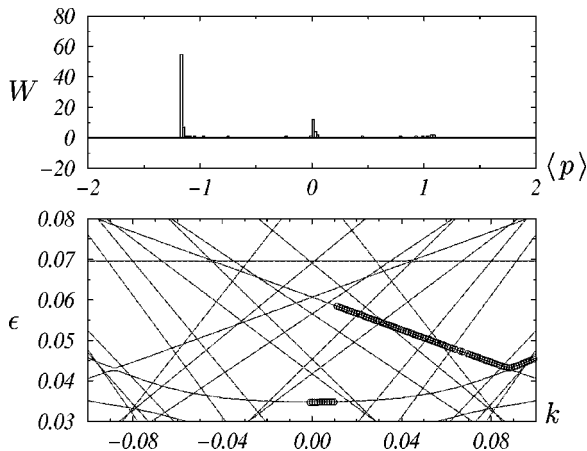


FIG. 13. The final states obtained after drift of the Bloch vector by  $\Delta k \approx 1/10$  (the initial state in Fig. 12). If the force governing the motion [Eq. (17)] is chosen such that the sliding is adiabatic through the avoided crossing at  $k=0$ , the momentum of the tunneling atoms just reverses its sign. If the initial states cover a small enough, well-centered, interval of the Brillouin zone, only the  $k=0$  avoided crossing is important. Other avoided crossings can be seen at  $k \approx \pm 0.09$  and  $\epsilon \approx 0.43$ . Those are responsible for the momentum dispersion of the atoms, and should be avoided as much as possible.

neled from  $\mathcal{I}_+$  to  $\mathcal{I}_-$  will end with a momentum close to  $-p_0$ . A standard time of flight technique should be enough to detect them. A more sophisticated technique, based for example, on velocity sensitive Raman transitions [54,48], could also be used with a subrecoil resolution if needed [24].

## VII. CONCLUSION

In this paper we have proposed a simple and accessible experimental configuration in which the observation of chaos-assisted tunneling should be feasible. It consists of atoms propagating in the light field of two far-detuned monochromatic standing waves with slightly different frequencies. However, observing the tunneling effect requires subrecoil cooling techniques to conveniently prepare the atomic sample together with a well-controlled experimental procedure (adiabatic preparation of the atomic state in one stable island followed by a drift of the Bloch vector). As the tunneling period fluctuates over several decades when the potential strength varies (see Fig. 8), observing that these fluctuations requires a stabilization of the laser intensity at the level of a few percent.

## ACKNOWLEDGMENTS

Ch.M., R.K., and A.M. would like to thank the Laboratoire Kastler Brossel for kind hospitality. CPU time on computers was provided by IDRIS. Laboratoire Kastler Brossel de l'Université Pierre et Marie Curie et de l'École Normale Supérieure is UMR 8552 du CNRS.

## APPENDIX A: DERIVATION OF THE EFFECTIVE HAMILTONIAN

To derive the effective Hamiltonian [Eq. 2], we basically proceed in three steps [55]. First we assume that any dissipation process can be safely ignored. Indeed for tunneling to be observable, the phase coherence of the atomic wave function must be preserved during all the process. In our case, this means that spontaneous emission must be negligible. It can be shown [56] that increasing the laser detuning considerably decreases the loss of phase coherence. Hence the evolution will be essentially Hamiltonian, provided that each laser beam is sufficiently far-detuned from the atomic resonance:

$$|\delta_{\pm}| = |\omega_{\pm} - \omega_{\text{at}}| \gg \Gamma. \quad (\text{A1})$$

When this holds, the total Hamiltonian operator for this two-level system is the sum of three terms: the kinetic energy operator describing the center-of-mass motion of atoms of mass  $M$ , the energy operator for the internal degrees of freedom, and the coupling between internal and external degrees of freedom. In the dipolar approximation, the interaction is just  $dE(x,t)$ , and it does not depend on  $y$  and  $z$ . The dynamics along  $y$  and  $z$  is just trivially described by free motion, and can be easily eliminated, since the total quantum state factorizes as a plane wave in  $y$  and  $z$ . One is then left with the dynamics along  $x$  which is described by the Hamiltonian

$$H_{\text{at}} = \frac{p_x^2}{2M} (|e\rangle\langle e| + |g\rangle\langle g|) + \hbar\omega_{\text{at}} |e\rangle\langle e| - dE(x,t) (|e\rangle\langle g| + |g\rangle\langle e|), \quad (\text{A2})$$

where  $p_x$  is the atomic momentum along  $x$ .  $|g\rangle$  and  $|e\rangle$  are the ground and excited states, and  $d$  is the atomic dipole strength connecting them.

Second, we expand the total atomic state as

$$|\Psi\rangle = \psi_g(x,t)|g\rangle + \psi_e(x,t)\exp(-i\omega_L t)|e\rangle, \quad (\text{A3})$$

and we neglect high frequency (optical) antiresonant terms and suppose that the amplitudes change slowly during an optical period. This is known as the rotating wave approximation [57], and features the averaging procedure to eliminate fast variables in classical perturbation theory [30]. This yields the coupled amplitude equations

$$i\hbar\partial_t\psi_g = -\frac{\hbar^2}{2M}\partial_{xx}^2\psi_g - \frac{\hbar\Omega(x,t)}{2}\psi_e, \quad (\text{A4a})$$

$$i\hbar\partial_t\psi_e = -\frac{\hbar^2}{2M}\partial_{xx}^2\psi_e - \hbar\delta_L\psi_e - \frac{\hbar\Omega^*(x,t)}{2}\psi_g. \quad (\text{A4b})$$

In these equations  $\delta_L = \omega_L - \omega_{\text{at}}$  is the mean laser detuning, the star denotes complex conjugation, and  $\Omega(x,t)$  reads

$$\Omega(x,t) = [\Omega_+ \exp(-i\delta\omega t/2) + \Omega_- \exp(i\delta\omega t/2)] \times \cos(k_L x), \quad (\text{A5})$$

where  $\Omega_{\pm} = dE_{\pm}/\hbar$  are the Rabi frequencies of each standing wave.

As a final step, we now assume that atoms initially prepared in their ground state mostly evolve in their ground state. This means that the whole atomic dynamics is solely determined by the ground-state amplitude  $\psi_g$ . For this to hold, an adiabatic elimination of the excited-state amplitude [56] must be justified. If the spatial partial derivatives were absent, Eqs. (A4) would just describe the Rabi oscillation phenomenon. It is then known that far off resonance, i.e., when the frequency separation of the states is much larger than any other frequencies, the Rabi oscillation is very small in amplitude. A sufficient condition is

$$|\delta_L| \gg \Omega_{\pm}, \delta\omega. \quad (\text{A6})$$

If, in addition, we assume that the excited-state kinetic energy is very small (which will be easily achieved with cold atoms),

$$|\delta_L| \gg \left\langle \psi_e \left| \frac{p_x^2}{2M} \right| \psi_e \right\rangle, \quad (\text{A7})$$

then an adiabatic elimination of the excited-state amplitude amounts to neglecting the spatial and temporal derivatives of  $\psi_e$  in Eq. A4b which is then solved as  $\psi_e \simeq -(\Omega^*/2\delta_L)\psi_g$

$\ll \psi_g$ . It is then easy to see that the ground-state amplitude  $\psi_g$  obeys an effective Schrödinger equation, with a Hamiltonian

$$H = \frac{p_x^2}{2M} + \frac{\hbar|\Omega(x,t)|^2}{4\delta_L}. \quad (\text{A8})$$

Eventually, up to an irrelevant purely time-dependent term, we obtain

$$H = \frac{p_x^2}{2M} - V_0 \cos(2k_L x) [\theta + \cos(\delta\omega t)], \quad (\text{A9})$$

where  $V_0 \stackrel{\text{def}}{=} -\hbar\Omega_+\Omega_-/8\delta_L$  and  $\theta \stackrel{\text{def}}{=} (\Omega_+/2\Omega_-) + (\Omega_-/2\Omega_+)$ .

## APPENDIX B: FLOQUET-BLOCH FORMALISM

In this appendix, we briefly recall the Floquet-Bloch formalism which is used for a quantum problem whose Hamiltonian  $H$  is periodic in both space and time. We will denote  $T$  and  $Q$  the temporal and spatial periods, respectively.

Let us first consider the time periodicity. We define [34,36,58]

$$K(\hat{p}, \hat{q}, \tau) \stackrel{\text{def}}{=} -i\hbar \frac{d}{d\tau} + H(\hat{p}, \hat{q}, \tau), \quad (\text{B1})$$

where  $\hat{p}$  and  $\hat{q}$  stand for canonical Hermitian operators whose commutator is  $[\hat{p}, \hat{q}] = -i\hbar$ .

If  $U(\tau', \tau)$  denotes the unitary evolution operator from  $\tau$  to  $\tau'$  associated with Hamiltonian  $H$ , the periodicity of the dynamics implies that  $U(\tau+T, T) = U(\tau, 0)$  and

$$U(\tau+T, \tau) = U(\tau+T, T)U(T, 0)U(0, \tau) = [U(0, \tau)]^{-1}U(T, 0)U(0, \tau). \quad (\text{B2})$$

This shows that  $U(\tau+T, \tau)$  and  $U(T, 0)$  differ by a unitary transformation, and hence have the same spectrum (but of course different eigenvectors), independent of  $\tau$ . The eigenvalues of  $U(\tau+T, \tau)$  have a unit modulus, and can be written as  $e^{-i\epsilon_n T/\hbar}$  where  $\epsilon_n$  is the so-called quasi-energy defined modulo  $2\pi\hbar/T$ . If  $|\psi_n(\tau)\rangle$  denotes the corresponding eigenvector, we can define the Floquet state

$$|\chi_n(\tau)\rangle \stackrel{\text{def}}{=} e^{i\epsilon_n \tau/\hbar} |\psi_n(\tau)\rangle, \quad (\text{B3})$$

which is by construction periodic with period  $T$ .

Inserting the definition of the Floquet state in the time-dependent Schrödinger equation, we immediately obtain

$$K(\hat{p}, \hat{q}, \tau) |\chi_n(\tau)\rangle = \epsilon_n |\chi_n(\tau)\rangle, \quad (\text{B4})$$

which means that the quasienergy spectrum is obtained by diagonalizing the Floquet Hamiltonian in the space of time-periodic functions.

The second step consists of making use of the invariance of  $H$  under spatial translations with period  $Q$ . The unitary

translation operator  $\hat{T}_Q \stackrel{\text{def}}{=} e^{-i\hat{p}Q/\hbar}$  commutes with  $K$ . We can then use the spatial counterpart of the Floquet theorem, namely, the Bloch theorem [33], and label the eigenstates of  $K$  with the Bloch number  $k \in [-\pi/Q, \pi/Q[$  (the first Brillouin zone), which means diagonalizing  $K$  in each subspace with fixed  $k$ . If one defines the Floquet-Bloch states as

$$|u_{n,k}(\tau)\rangle = e^{-ik\hat{q}}|\chi_{n,k}(\tau)\rangle = e^{i\epsilon_n(k)\tau/\hbar} e^{-ik\hat{q}}|\psi_{n,k}(\tau)\rangle, \quad (\text{B5})$$

where  $\{\psi_{n,k}(\tau)\}$  forms a complete orthogonal eigenbasis, it is easy to show that they can be obtained by diagonalizing the Floquet-Bloch Hamiltonian,

$$\tilde{K}(\hat{p}, \hat{q}, \tau, k) = K(\hat{p} + \hbar k, \hat{q}, \tau), \quad (\text{B6})$$

on the subspace of time and space periodic functions. In our specific case, the Floquet-Bloch Hamiltonian reads

$$\tilde{K}(\hat{p}, \hat{q}, \tau, k) = \frac{(\hat{p} + \hbar k)^2}{2} - \gamma(\theta + \cos \tau) \cos \hat{q} - i\hbar \frac{d}{d\tau}. \quad (\text{B7})$$

The spatial periodicity of the Floquet-Bloch states leads to a discrete set of dispersion relations  $\epsilon_n(k)$ . For fixed  $n$ , the set of all quasienergies  $\epsilon_n(k)$  for  $k$  in the first Brillouin zone  $[-\pi/Q, \pi/Q[$  is called the  $n$ th band of the system.

Let us now obtain the velocity theorem [Eq. 10]. Using the above relations, we have

$$\begin{aligned} \langle \psi_{\epsilon,k}(\tau) | \hat{p} | \psi_{\epsilon,k}(\tau) \rangle &= \langle u_{\epsilon,k}(\tau) | (\hat{p} + \hbar k) | u_{\epsilon,k}(\tau) \rangle \\ &= \langle u_{\epsilon,k}(\tau) | (\hbar^{-1} \partial \tilde{K} / \partial k) | u_{\epsilon,k}(\tau) \rangle. \end{aligned}$$

The derivation with respect to  $k$  of the relation  $\langle u_{\epsilon,k}(\tau) | \tilde{K} | u_{\epsilon,k}(\tau) \rangle = \epsilon(k)$  leads to

$$\begin{aligned} \langle \psi_{\epsilon,k}(\tau) | \hat{p} | \psi_{\epsilon,k}(\tau) \rangle &= \frac{1}{\hbar} \frac{\partial \epsilon}{\partial k} + i\hbar \frac{d}{d\tau} \left( \langle u_{\epsilon,k}(\tau) | \frac{\partial}{\partial k} | u_{\epsilon,k}(\tau) \rangle \right) \\ &\quad - \left( \frac{1}{\hbar} \frac{\partial}{\partial k} \langle u_{\epsilon,k}(\tau) | \tilde{K} | u_{\epsilon,k}(\tau) \rangle \right) \\ &\quad - \left[ \left( \frac{1}{\hbar} \frac{\partial}{\partial k} \langle u_{\epsilon,k}(\tau) | \tilde{K} | u_{\epsilon,k}(\tau) \rangle \right)^* \right]. \end{aligned} \quad (\text{B8})$$

The two last terms on the the right hand side are opposite, since the normalization of the  $u$ 's leads to  $\partial \langle u_{\epsilon,k} | u_{\epsilon,k} \rangle / \partial k = 0$ . Moreover, after time averaging Eq. B8 over  $T$ , the total  $\tau$  derivative vanishes since the  $u$ 's are precisely  $T$  periodic while the time-independent  $k$  derivative of the quasienergy remains unchanged. Eventually,

$$\frac{1}{T} \int_0^T \langle \psi_{\epsilon,k}(\tau) | \hat{p} | \psi_{\epsilon,k}(\tau) \rangle d\tau = \frac{1}{\hbar} \frac{\partial \epsilon}{\partial k}. \quad (\text{B9})$$

### APPENDIX C: BLOCH ANGLE DYNAMICS

In this appendix we derive Eq. (17), which is valid for an arbitrary strength of the constant force  $F$  provided that the potential  $V = -Fq$  remains strictly linear in  $q$ . Let us choose a state  $|\psi(\tau)\rangle$  evolving under  $H' = H + V$ , such that it coincides with a Floquet-Bloch state at  $\tau = 0$ :

$$i\hbar_{\text{eff}} \frac{d|\psi(\tau)\rangle}{d\tau} = H'(\hat{p}, \hat{q}, \tau) |\psi(\tau)\rangle \quad (\text{C1})$$

and

$$|\psi(\tau=0)\rangle = |\psi_{n,k}(\tau=0)\rangle. \quad (\text{C2})$$

In the interaction picture, we immediately have

$$i\hbar_{\text{eff}} \frac{d|\psi^I(\tau)\rangle}{d\tau} = -FU^\dagger(\tau, 0) \hat{q} U(\tau, 0) |\psi^I(\tau)\rangle, \quad (\text{C3})$$

where  $|\psi^I(\tau)\rangle \stackrel{\text{def}}{=} U^\dagger(\tau, 0) |\psi(\tau)\rangle$ , and where  $U$  denotes the evolution operator under  $H$ . Let  $|\phi(\tau)\rangle$  be the ket defined by

$$|\phi(\tau)\rangle \stackrel{\text{def}}{=} e^{-iF\hat{q}\tau/\hbar_{\text{eff}}} |\psi^I(\tau)\rangle. \quad (\text{C4})$$

It is straightforward to obtain its evolution,

$$i\hbar_{\text{eff}} \frac{d|\phi(\tau)\rangle}{d\tau} = G(\tau) |\phi(\tau)\rangle, \quad (\text{C5})$$

where

$$G(\tau) \stackrel{\text{def}}{=} F(\hat{q} - e^{-i\tau F\hat{q}/\hbar_{\text{eff}}} U^\dagger(\tau, 0) \hat{q} U(\tau, 0) e^{i\tau F\hat{q}/\hbar_{\text{eff}}}). \quad (\text{C6})$$

Since  $U^\dagger(\tau, 0)$  commutes with the translation operator  $\hat{T}_Q$ , it can be checked that  $[G(\tau), \hat{T}_Q] = 0$ . The evolution of  $|\phi(\tau)\rangle$  under  $G$  will therefore preserve its initial quantum number  $k$ ,

$$\hat{T}_Q |\phi(\tau)\rangle = e^{-ikQ} |\phi(\tau)\rangle, \quad (\text{C7})$$

for all  $\tau$ . Thus, making use of Eqs. (C3) and (C4), we have

$$\hat{T}_Q |\psi(\tau)\rangle = e^{-i(k + F\tau/\hbar_{\text{eff}})Q} |\psi(\tau)\rangle, \quad (\text{C8})$$

which shows that  $|\psi(\tau)\rangle$  is actually a Bloch wave with a Bloch angle given by  $k(\tau) = k(0) + F\tau/\hbar_{\text{eff}}$ , even if it spreads among the quasienergy bands [39,38].

- [1] *Chaos et Physique Quantique—Chaos and Quantum Physics*, Les Houches, École d'été de Physique Théorique 1989, Session LII, edited by M. Giannoni, A. Voros, and J. Zinn-Justin (North-Holland, Amsterdam, 1991).
- [2] E.J. Heller, Phys. Rev. Lett. **53**, 1515 (1984).
- [3] *Mesoscopic Quantum Physics*, Les Houches, École d'été de Physique Théorique 1994, Session LXI, edited by E. Akkermans, G. Montambaux, J. Pichard, and J. Zinn-Justin (North-Holland, Amsterdam, 1995), session LXI.
- [4] A. Messiah, *Mécanique Quantique* (Dunod, Paris, 1964), Vol. 2.
- [5] R. Balian and C. Bloch, Ann. Phys. (N.Y.) **84**, 559 (1974).
- [6] M. Wilkinson, Physica D **21**, 341 (1986).
- [7] M. Wilkinson and J.H. Hannay, Physica D **27**, 201 (1987).
- [8] W.A. Lin and L.E. Ballentine, Phys. Rev. Lett. **65**, 2927 (1990).
- [9] O. Bohigas, D. Boosé, R. Eydio de Carvalho, and V. Marville, Nucl. Phys. A **560**, 197 (1993).
- [10] O. Bohigas, S. Tomsovic, and D. Ullmo, Phys. Rep. **223**, 43 (1993).
- [11] S. Tomsovic and D. Ullmo, Phys. Rev. E **50**, 145 (1994).
- [12] S.C. Creagh and N.D. Whelan, Phys. Rev. Lett. **77**, 4975 (1996).
- [13] V. Averbukh, N. Moiseyev, B. Mirbach, and H.J. Korsh, Z. Phys. D: At., Mol. Clusters **35**, 247 (1995).
- [14] *Laser and Manipulation of Atoms and Ions*, Enrico Fermi International Summer School, 1991, Course CXVIII, edited by E. Arimondo, W.D. Phillips, and F. Strumia (North-Holland, Amsterdam, 1992).
- [15] R.T. Lawton and M.S. Child, Mol. Phys. **44**, 709 (1981).
- [16] E.L. Sibert, W.P. Reinhardt, and J.T. Hynes, Chem. Phys. Lett. **92**, 455 (1982).
- [17] M.E. Kellman and E.D. Lynch, Chem. Phys. **87**, 5386 (1987).
- [18] J.P. Rose and M.E. Kellman, J. Chem. Phys. **105**, 7348 (1996).
- [19] J.P. Rose and M.E. Kellman, J. Chem. Phys. **105**, 10743 (1996).
- [20] *Atom Interferometry*, edited by P.R. Berman (Academic Press, New York, 1996).
- [21] M. Weidemüller, A. Hemmerich, A. Görlitz, T. Esslinger, and T.W. Hänsch, Phys. Rev. Lett. **75**, 4583 (1995).
- [22] L. Guidoni, C. Triché, P. Verkerk, and G. Grynberg, Phys. Rev. Lett. **79**, 3363 (1997).
- [23] K. Drese and M. Holthaus, Phys. Rev. Lett. **78**, 2932 (1997).
- [24] M. Ben Dahan, E. Peik, J. Reichel, Y. Castin, and C. Salomon, Phys. Rev. Lett. **76**, 4508 (1996).
- [25] Q. Niu, X.-G. Zhao, G.A. Georgakis, and M.G. Raizen, Phys. Rev. Lett. **76**, 4504 (1996).
- [26] F.L. Moore, J.C. Robinson, C. Bharucha, P.E. Williams, and M.G. Raizen, Phys. Rev. Lett. **73**, 2974 (1994).
- [27] G. Labeyrie, F. de Tomasi, J.C. Bernard, C.A. Müller, C. Miniatura, and R. Kaiser, Phys. Rev. Lett. **83**, 5266 (1999).
- [28] T. Jonckheere, C.A. Müller, R. Kaiser, C. Miniatura, and D. Delande, Phys. Rev. Lett. **85**, 4269 (2000).
- [29] C. Cohen-Tannoudji, J. Dupont-Roc, and G. Grynberg, *Processus d'Interaction entre Photons et Atomes, Savoirs Actuels* (InterEditions/Éditions du CNRS, Paris, 1988).
- [30] A.J. Lichtenberg and M.A. Lieberman, *Regular and Stochastic Motion*, Applied Mathematical Sciences Vol. 38 (Springer-Verlag, New York, 1983).
- [31] B. Chirikov, Phys. Rep. **52**, 263 (1979).
- [32] M.J. Davis and E.J. Heller, J. Phys. Chem. **85**, 307 (1981).
- [33] N.W. Ashcroft and N.D. Mermin, *Solid State Physics* (Saunders College, Philadelphia, 1976).
- [34] G. Floquet, Ann. de l'Éc. Normale, 2<sup>e</sup> Sér. **12**, 47 (1883) (in French).
- [35] T.M. Cherry, Proc. London Math. Soc. (2nd ser.) **26**, 211 (1927).
- [36] J.H. Shirley, Phys. Rev. **138**, B979 (1965).
- [37] W.H. Louisell, *Quantum Statistical Properties of Radiation* (Wiley, Chichester, 1973).
- [38] J. von Neumann and E. Wigner, Phys. Z. **30**, 467 (1929). English translation in *Symmetry in the Solid State* (Ref. [60]), pp. 167–172.
- [39] P. Leboëuf and A. Voros, in *Quantum Chaos—Between Order and Disorder*, edited by G. Casati and B. Chirikov (Cambridge University Press, Cambridge, 1992), pp. 507–533. See *Quantum Chaos—Between Order and Disorder* (Ref. [59]).
- [40] E.M. Zanardi, J. Gutiérrez, and J.M. Gomez Llorente, Phys. Rev. E **52**, 4736 (1995).
- [41] J. Zakrzewski, D. Delande, and A. Buchleitner, Phys. Rev. E **57**, 1458 (1998).
- [42] S. Washburg and R. Webb, Adv. Phys. **35**, 375 (1986).
- [43] S. Feng and P.A. Lee, Science **251**, 633 (1991).
- [44] F. Leyvraz and D. Ullmo, J. Phys. A **29**, 2529 (1996).
- [45] J. Zakrzewski and D. Delande, Phys. Rev. E **47**, 1650 (1993).
- [46] J.-P. Bouchaud and A. Georges, Phys. Rep. **195**, 127 (1990).
- [47] R. Roncaglia, L. Bonci, F.M. Izrailev, B.J. West, and P. Grigolini, Phys. Rev. Lett. **73**, 802 (1994).
- [48] M. Morinaga, I. Bouchoule, J.-C. Karam, and C. Salomon, Phys. Rev. Lett. **83**, 4037 (1999).
- [49] M. Kasevich and S. Chu, Phys. Rev. Lett. **69**, 1741 (1992).
- [50] J. Reichel, F. Bardou, M. Ben Dahan, E. Peik, S. Rand, C. Salomon, and C. Cohen-Tannoudji, Phys. Rev. Lett. **75**, 4575 (1995).
- [51] M. Abramowitz and I.A. Stegun, *Handbook of Mathematical Functions* (Dover, New York, 1965).
- [52] J. Callaway, *Quantum Theory of the Solid State* (Academic Press, London, 1974), Vol. B.
- [53] C. Zener, Proc. R. Soc. London, Ser. A **137**, 696 (1932).
- [54] V. Vuletić, C. Chin, A.J. Kerman, and S. Chu, Phys. Rev. Lett. **81**, 5768 (1998).
- [55] R. Graham, M. Schlautmann, and P. Zoller, Phys. Rev. A **45**, R19 (1992).
- [56] C. Cohen-Tannoudji, in *Systèmes Fondamentaux en Optique Quantique — Fundamental Systems in Quantum Optics*, Les Houches, École d'été de Physique Théorique 1990, Session LIII, edited by J. Dalibard, J.-M. Raimond, and J. Zinn-Justin (North-Holland, Amsterdam, 1990), pp. 1–164.
- [57] A.L.C. and J. Eberly, *Optical Resonance and Two Level Atoms* (Dover, New York, 1987).
- [58] Y.B. Zeldovich, Zh. Éksp. Fiz. **51**, 1492 (1966) [Sov. Phys. JETP **24**, 1006 (1967)].
- [59] *Quantum Chaos—Between Order and Disorder*, edited by G. Casati and B. Chirikov (Cambridge University Press, Cambridge, 1995).
- [60] R.S. Knox and A. Gold, *Symmetry in the Solid State*, Lecture Notes and Supplements in Physics (Benjamin, New York, 1964).